Future Engineering in ELECTRICAL, ELECTRONICS, and COMMUNICATION SYSTEMS

Editör
Ali Can Çabuker

BİDGE

BİDGE Yayınları

Future Engineering in Electrical, Electronics, and Communication Systems

Editor: ALİ CAN ÇABUKER

ISBN: 978-625-8567-07-6

1st Edition
Page Layout By: Gözde YÜCEL
Publication Date: 2025-12-25
BİDGE Yayınları

Certificate No: 71374

www.bidgeyayinlari.com.tr - bidgeyayinlari@gmail.com
Krc Bilişim Ticaret ve Organizasyon Ltd. Şti.
Güzeltepe Mahallesi Abidin Daver Sokak Sefer Apartmanı No: 7/9 Çankaya / Ankara

PREFACE

The accelerating evolution of engineering technologies has diminished the clear distinctions between conventional disciplines, giving rise to highly integrated and multifaceted systems that demand interdisciplinary perspectives. This book presents a collection of recent theoretical advances and real-world implementations spanning electromagnetic, microwave, and radio-frequency technologies, intelligent sensing systems, modern communication infrastructures, artificial intelligence, electric mobility, and advanced control techniques. By uniting contributions from a wide range of engineering domains, the book offers a holistic view of emerging technologies that are driving innovation in medical, industrial, and transportation applications. Intended for researchers, undergraduate and graduate students, and stakeholders across the engineering ecosystem, this volume emphasizes the critical role of interdisciplinary collaboration in addressing modern engineering problems and fostering the development of intelligent, high-performance, and sustainable technological solutions.

Asst. Prof. Ali Can ÇABUKER

ARTVİN ÇORUH UNIVERSITY

İÇİNDEKİLER

CHAPTER 1

INNOVATIVE APPLICATIONS OF MICROWAVE AND RADIOFREQUENCY TECHNOLOGIES IN MEDICAL DIAGNOSIS AND THERAPY

LEVENT SEYFİ[1]

Introduction

This chapter provides an exhaustive examination of the rapidly evolving intersection of microwave (MW) and radiofrequency (RF) engineering with clinical medicine. It delves beyond a superficial overview to present a detailed technical and clinical analysis of non-ionizing electromagnetic technologies reshaping diagnostic imaging, therapeutic intervention, and personalized health monitoring. The discourse begins with a rigorous foundation in the dielectric and thermal response of biological tissues across the RF/MW spectrum. It subsequently offers a critical, in-depth review of microwave imaging systems, contrasting radar-based and tomography-based architectures for breast and brain applications. A thorough analysis of thermal therapy follows, comparing the physics, efficacy, and technological evolution of RF and microwave ablation alongside focused

[1] Prof.Dr., Konya Teknik Üniversitesi, Elektrik Elektronik Mühendisliği Bölümü, Orcid: 0000-0002-8698-5140

hyperthermia systems. The chapter dedicates significant attention to the specialized field of biomedical antenna design, addressing the unique challenges of implantable and wearable devices, including biocompatibility, miniaturization, and on-body performance. A paramount emphasis is placed on safety protocols, specifically the computational and experimental methodologies for Specific Absorption Rate (SAR) evaluation and optimization. The indispensable role of advanced numerical phantoms and tissue-equivalent materials in system validation is detailed. The chapter candidly addresses the multifaceted pathway to clinical adoption, including regulatory hurdles, clinical trial design, and workflow integration. Finally, it synthesizes a forward-looking perspective on how metamaterial-enabled devices and artificial intelligence (AI) algorithms are poised to fundamentally disrupt and enhance the capabilities of next-generation medical RF/MW systems, paving the way for truly adaptive and intelligent therapeutic and diagnostic platforms.

The Electromagnetic Foundations of Biological Interaction

The therapeutic and diagnostic application of microwave (MW) and radiofrequency (RF) energy is intrinsically predicated upon the quantifiable interaction between propagating electromagnetic fields and heterogeneous, dissipative biological media. This interaction, distinct from ionizing radiation, is primarily characterized by dielectric polarization and conductive loss mechanisms, culminating in energy deposition and temperature elevation.

At a fundamental level, the macroscopic response of tissue is described by its complex relative permittivity,

$$\varepsilon_r^* = \varepsilon_r' - j\varepsilon_r''$$

where the real part (ε_r') signifies the ability to store electrical energy (polarization), and the imaginary part (ε_r'') encapsulates both

dielectric relaxation losses and losses due to ionic conductivity (σ), related by $\varepsilon_r'' = \frac{\sigma}{(\omega\, \varepsilon_0)}$ (Gabriel et al., 1996). The frequency dispersion of these parameters from kHz to GHz, characterized by prominent α, β, and γ dispersions, is critical for technology design (Foster and Schwan, 1989). The penetration depth (δ), defined as the distance over which the field amplitude decreases by a factor of $1/e$, is approximated by

$$\delta \approx 1/\sqrt{\{\pi f \mu \sigma\}}$$

for conductive tissues, establishing a fundamental engineering trade-off: lower frequencies (e.g., 100-500 MHz for RF ablation) penetrate deeper but offer poorer spatial resolution, while higher frequencies (e.g., 1-10 GHz for microwave imaging) provide finer resolution but suffer from increased attenuation (Brace, 2011).

The thermal effect, the basis for most therapies, is governed by the bioheat transfer equation, with the local volumetric heat generation rate (Q) described by $Q = \frac{1}{2}\, \sigma\, |E|^2$ (Joule heating, dominant at RF) or more generally by $Q = \frac{1}{2}\, \omega \varepsilon_0 \varepsilon_r'' |E|^2$ (dielectric heating, dominant at MW). The resulting temperature rise can induce reversible hyperthermic sensitization (40-45°C) or irreversible coagulative necrosis (>50-60°C) (Miklavčič, 2017). For diagnostic imaging, the dielectric contrast between tissues is the key source of information. Malignant breast tissues, for instance, have been consistently shown to exhibit significantly higher ε_r' and σ than adjacent healthy fibroglandular or adipose tissues across the 0.5-10 GHz range, due to increased water content and cellularity (Lazebnik et al., 2007). This intrinsic contrast provides the physical basis for tumor detection without exogenous contrast agents. A nuanced understanding of these electromagnetic-thermal-tissue relationships is therefore the indispensable first step in innovating safe, effective, and targeted medical devices (O'Rourke et al., 2007).

Microwave Imaging Systems: From Principles to Clinical Prototypes

Microwave Imaging (MWI) leverages the dielectric contrast described above to reconstruct anatomical or functional maps of the body. It presents a compelling alternative to modalities like X-ray mammography (ionizing) and MRI (high-cost), particularly for specific applications. The field is broadly divided into two algorithmic approaches: radar-based and tomography-based.

Radar-Based Microwave Imaging: This approach treats the imaging problem as a target detection and localization task. A short ultrawideband (UWB) pulse is transmitted, and backscattered signals from dielectric discontinuities are collected. Techniques like confocal microwave imaging (CMI) or delay-and-sum (DAS) beamforming are used to synthetically focus on every point within the region, creating a reflectivity map (Fear et al, 2003). Its strengths are computational simplicity and robustness. It is highly effective for detecting strong scatterers like tumors but provides less quantitative tissue property information.

Tomography-Based Microwave Imaging (MWT): This is a quantitative, inverse scattering approach. It aims to reconstruct the complete spatial distribution of ε_r' and σ by solving a nonlinear, ill-posed optimization problem that minimizes the difference between measured and simulated scattered fields (Meaney et al, 2000). While computationally intensive and sensitive to modeling errors, it offers the potential for true dielectric property mapping, which could aid in tissue characterization (e.g., differentiating benign from malignant) (Cetinkaya, 2025).

Clinical Applications:

a. Breast Cancer Screening and Diagnosis: MWI for the breast is the most advanced application. Systems like the MIT system (tomographic) and the MSI system from

McGill/University of Calgary (radar) have undergone extensive clinical studies (Porter et al, 2013). Results indicate high sensitivity, especially in dense breasts where mammography sensitivity drops. Recent advances focus on 3D imaging, multi-frequency data fusion, and integration with compression plates to improve image quality and patient comfort (Nikolova, 2011).

b. Cerebral Imaging (Stroke Detection): The urgent need for rapid, bedside stroke differentiation drives MWI research for the brain. The main challenge is the complex, multilayered structure of the head (skin, skull, CSF, brain). Advanced forward models and compensation algorithms for the high-contrast skull are critical (Mustafa et al, 2013). Prototype helmet-like arrays are being developed for continuous monitoring in emergency rooms or ambulances (Tobon Vasquez et al, 2020).

c. Functional and Other Applications: Emerging areas include monitoring of brain temperature or edema, imaging for joint inflammation (arthritis), and bone health assessment (Shevelev et al., 2022; Laskari et al., 2023; Shakhawat Hossen et al.,2024).

RF Ablation, Microwave Ablation, and Hyperthermia: A Comparative Therapeutic Arsenal

Thermal ablation has revolutionized the minimally invasive treatment of inoperable tumors. While sharing the goal of thermal necrosis, RF and MW ablation differ fundamentally in physics, performance, and clinical indications.

Radiofrequency Ablation (RFA): As the historical gold standard, RFA employs frequencies between 375-500 kHz. An alternating current propagates from a needle electrode through the ionic tissue, causing resistive (Joule) heating. The extent of ablation

is limited by electrical impedance, which rises sharply as tissue desiccates and chars (~100°C), creating an insulating barrier that restricts further current flow and limits ablation zone size (typically < 3-4 cm). Multipronged or cooled-tip electrodes were developed to mitigate this (Haemmerich and Schutt, 2011). RFA remains highly effective for smaller tumors (<3 cm) in organs like the liver, kidney, and bone.

Microwave Ablation (MWA): Operating at 915 MHz or 2.45 GHz (ISM bands), MWA delivers energy via an antenna that emits an electromagnetic field. Heating occurs through the rotation of water molecules (dielectric loss), which is a more efficient and volumetric process. Key advantages over RFA include: 1) Faster heating and higher intratumoral temperatures; 2) Larger ablation volumes (>5 cm possible with single antenna); 3) Less susceptibility to heat sink effects from nearby blood vessels; 4) Efficacy in charred or cystic tissues (does not rely on conductivity) (Brace, 2009). Technological advancements focus on antenna design to shape the ablation zone (e.g., choked, triaxial, or slot-loaded antennas for more spherical profiles), multi-antenna synchronous systems for large volumes, and real-time temperature monitoring integration (Zhang et al., 2025; Jin et al., 2025; Fang, 2025).

Focused RF/MW Hyperthermia: This adjuvant therapy aims for a moderate, uniform temperature rise (40-45°C) within a tumor to increase its sensitivity to radiation or chemotherapy. It requires sophisticated phased-array applicators (e.g., annular phased arrays, waveguide arrays) that can electronically steer and focus energy deep inside the body. The technical challenge is to overcome focusing limitations in heterogeneous tissue. Treatment planning systems using patient-specific CT/MRI data are used to optimize phase and amplitude settings for each antenna element to maximize the therapeutic index (Wust et al., 2002). Clinical evidence supports

its benefit in cancers of the cervix, rectum, and soft tissue sarcomas (Van Rhoon et al, 2013).

Advanced Antenna Design for Implantable and Wearable Biomedical Devices

The antenna is the critical interface between electronic medical devices and the biological environment or external world. Its design is governed by a unique set of constraints that diverge sharply from conventional free-space antenna theory.

Implantable Antennas: Devices such as cardiac pacemakers, deep brain stimulators (DBS), gastric monitors, and biodegradable sensors require antennas that are miniaturized, biocompatible, and stable within the lossy, high-permittivity tissue medium. Key challenges include:

a. Extreme Miniaturization: Strategies include fractal geometries, meander lines, spiral designs, and the use of high-permittivity ceramic substrates ($\varepsilon_r > 10$) which reduce the guided wavelength, allowing for smaller resonant structures (Kiourti and Nikita, 2012).

b. Biocompatibility and Hermetic Sealing: The antenna must be electrically insulated from the host tissue to prevent corrosion and biofouling, typically using bioglass, alumina (Al_2O_3), or medical-grade polymers like PEEK or PDMS. This encapsulant layer significantly detunes the antenna, necessitating co-design.

c. Robust Performance in Tissue: The near-field is dominated by the surrounding tissue properties. Design optimization must be performed using numerical models with realistic tissue layers.

Bandwidth is often prioritized to accommodate frequency shifts due to variable tissue encapsulation thickness or composition (Nikita, 2014).

d. Safety (Low SAR): The antenna must be designed to operate with minimal near-field heating, adhering to strict SAR limits for implanted devices.

Wearable and On-Body Antennas: Used in smart health patches, continuous glucose monitors, EEG/ECG sensors, and Body Area Networks (BANs). Primary considerations are:

a. Flexibility and Conformality: Antennas must bend and stretch with skin movement without performance degradation. This is achieved using flexible substrates (polyimide, PET, textile) and conductive materials like silver ink, conductive thread, or liquid metal alloys (e.g., Galinstan) (Koul and Bharadwaj, 2021; Yurduseven et al, 2018).

b. Detuning and Body Coupling: The antenna's input impedance and radiation pattern are severely distorted when placed on the body. Techniques to mitigate this include incorporating a metallic ground plane as a reflector (also reduces SAR), using electromagnetic band-gap (EBG) or artificial magnetic conductor (AMC) surfaces to create an in-phase reflective boundary, and designing specific "on-body" matching networks (Ashyap et al., 2025).

c. Specific Absorption Rate (SAR) Management: For devices operating near the body, minimizing backward radiation is crucial. Directional antennas (e.g., planar inverted-F antennas - PIFAs) and the aforementioned EBG structures are effective in lowering peak spatial SAR.

d. Durability: Wearable antennas must withstand washing, sweat, and mechanical wear. Encapsulation and robust material choices are essential.

Comprehensive Safety Assessment and SAR Optimization Methodologies

Ensuring patient safety is the non-negotiable cornerstone of any medical RF/MW application. The Specific Absorption Rate (SAR), defined as the time derivative of the incremental energy absorbed by an incremental mass in a tissue volume ($SAR = \frac{d}{dt}\left(\frac{dW}{dm}\right) = \frac{\sigma}{\rho}|E|^2$), is the primary dosimetric quantity for assessing exposure.

Regulatory Limits and Standards: International guidelines, notably from the International Commission on Non-Ionizing Radiation Protection (ICNIRP) and the Institute of Electrical and Electronics Engineers (IEEE), define basic restrictions for localized and whole-body SAR. For example, IEEE C95.1-2019 sets a localized SAR limit of $2\ W/kg$ averaged over any $10\ g$ of tissue in the head and trunk for the general public, with higher limits for extremities and occupational exposure (IEEE Std, 2019). Medical devices must demonstrate compliance through rigorous testing.

Computational SAR Evaluation: Numerical simulation using anatomically detailed human models (e.g., "Duke," "Ella," "Norman" from the IT'IS Foundation) and Finite-Difference Time-Domain (FDTD) or Finite Element Method (FEM) solvers is the standard for predictive safety analysis. It allows for 3D volumetric SAR mapping under various exposure scenarios before physical prototyping (Christ et al., 2010). Key outputs include peak spatial-average SAR (psSAR) and its distribution.

SAR Optimization Strategies:

a. For Therapeutic Devices (Ablation/Hyperthermia): The goal is to maximize SAR in the target volume while minimizing it in healthy tissue. This involves:

- Antenna/Applicator Design: Shaping the near-field pattern (e.g., using multi-slot antennas for more spherical ablation).
- Phased-Array Focusing: Using multiple applicators with optimized amplitude and phase control to constructively interfere at the target. This is the basis for deep-heating hyperthermia systems (Nguyen, 2017).
- Robust Treatment Planning: Using optimization algorithms (e.g., particle swarm, convex optimization) with patient-specific models to calculate driving signals.

b. For Diagnostic/Wearable Devices: The goal is to minimize SAR while maintaining functional link budget or image quality.

- Antenna Design: Employing directional designs (PIFA, patch with EBG) to reduce energy directed into the body.
- Power Management: Implementing duty cycling and adaptive power control.
- Array Excitation Optimization: In MWI, using low-SAR illumination patterns that still provide sufficient information for image reconstruction.

Experimental SAR Measurement: Validation is performed in tissue-equivalent liquid phantoms using robotic SAR probes (e.g., isotropic electric field probes) that scan the area of interest according to standardized protocols (e.g., IEC 62209) (Burkhardt and Kuster, 2000; International, 2020).

Anthropomorphic Phantoms: Bridging Simulation and Clinical Reality

Phantoms are physical or numerical models that mimic the electromagnetic or thermal properties of human tissues. They are indispensable for device development, calibration, performance validation, and safety testing, serving as a crucial bridge between computational models and in vivo applications.

Numerical (Digital) Phantoms: These are 3D computer models with assigned tissue properties.

a. Voxel Models: Derived from high-resolution MRI or CT scans (e.g., "Virtual Family," "AustinMan"), they provide unparalleled anatomical realism but have discrete tissue boundaries (ITIS, 2025).

b. Surface-Based Models: Composed of smooth triangular meshes, often derived from the same medical images, they are better suited for certain numerical methods like FEM. These models enable virtual clinical trials, allowing for statistical analysis of device performance across a population with different anatomies.

Physical Tissue-Equivalent Phantoms: These are fabricated materials with controlled dielectric properties (ε_r', σ).

a. Liquid Phantoms: Homogeneous mixtures of water, salt, sugar, and hydrogel-forming agents (e.g., TX-151, agar). They are ideal for SAR measurement and antenna testing in standardized geometries (e.g., SAM head) (Deng et al., 2025).

b. Gel/Solid Phantoms: Using agents like agar, gelatin, or polyacrylamide, these can be molded into shapes. They are used for imaging phantoms (e.g., breast

phantoms with embedded tumor simulants) and ablation validation.

c. Anatomically Realistic Phantoms: Advances in 3D printing and molding enable the creation of phantoms with realistic external shapes and internal heterogeneous structures. Multi-material 3D printing allows for spatial variation of dielectric properties, a significant step forward (Bai et al., 2025).

d. Dynamic and Thermal Phantoms: For ablation studies, phantoms that mimic the temperature-dependent dielectric properties of tissue or that allow for thermographic mapping of ablation zones are under development (Bublex, et al., 2025; Meaney et al., 2025).

The development of accurate, stable, and reproducible phantoms across a broad frequency range remains an active research area critical for standardizing performance evaluation across different research groups and for regulatory submissions.

The Pathway to Clinical Adoption: Regulatory, Economic, and Practical Hurdles

Translating a promising engineering prototype into a clinically adopted, commercially viable medical device is a complex, resource-intensive journey fraught with non-technical challenges.

Regulatory Approval: In the United States, devices are regulated by the Food and Drug Administration (FDA) under classifications (Class I, II, III) based on risk. Most RF/MW therapeutic devices (ablation systems) are Class II (510(k) clearance) or Class III (Premarket Approval - PMA), requiring demonstration of substantial equivalence to a predicate device or extensive clinical data proving safety and effectiveness, respectively (U.S. Food,

2025). In the European Union, the Medical Device Regulation (MDR) 2017/745 requires a conformity assessment by a Notified Body. The regulatory dossier must include detailed technical files, risk management reports (ISO 14971), biocompatibility data (ISO 10993), electromagnetic compatibility (EMC) reports, and crucially, clinical evaluation reports.

Clinical Trial Design: Generating high-quality clinical evidence is the most significant hurdle. Trials must be meticulously designed to answer specific clinical questions (e.g., non-inferiority to the standard of care for an ablation device, or sensitivity/specificity for an imaging system). Challenges include patient recruitment, defining appropriate endpoints (e.g., technical success vs. overall survival), and managing confounding variables. For novel imaging systems like MWI, establishing the "ground truth" for comparison (e.g., MRI or biopsy) is essential but can be logistically difficult (Adachi, 2021).

Reimbursement: Even with regulatory approval, adoption hinges on reimbursement from healthcare payers (e.g., Medicare in the US). This requires the establishment of a Current Procedural Terminology (CPT) code and demonstration of clinical utility and cost-effectiveness compared to existing alternatives. This economic argument is often as important as the technical one.

Integration into Clinical Workflow: A device must be user-friendly, reliable, and fit seamlessly into existing hospital workflows. Complex systems requiring lengthy setup, specialized operators, or significant additional training will face resistance. Reliability, serviceability, and cost of consumables are key practical considerations (Vilaça, 2020; Leong et al, 2024).

Frontiers of Innovation: Metamaterials and Artificial Intelligence

The convergence of RF/MW engineering with metamaterials (MTMs) and artificial intelligence (AI) is defining the next technological frontier, promising breakthroughs in performance, functionality, and autonomy.

Metamaterials for Enhanced Devices: MTMs are artificial structures with sub-wavelength unit cells that exhibit extraordinary electromagnetic properties not found in nature (e.g., negative refractive index, near-zero permittivity).

a. Super-Resolution Imaging: MTM lenses or "superlenses" can overcome the diffraction limit, potentially enabling microwave imaging with resolutions approaching the millimeter scale, rivaling ultrasound (Engheta and Ziolkowski, 2006).

b. Miniaturized and Efficient Antennas: MTM-inspired structures (e.g., metasurfaces) can be used as substrates or superstrates to dramatically reduce antenna size, enhance bandwidth, or improve isolation between elements in dense arrays for MWI or hyperthermia (Kumar et al., 2021; El Houda Nasri, et al., 2025).

c. Smart Skins and Dynamic Apertures: Reconfigurable metasurfaces, whose properties can be tuned electronically, could lead to wearable imaging systems or adaptive hyperthermia applicators that can focus energy dynamically in response to patient movement or tissue changes (Cai et al., 2025; Pang, 2025).

Artificial Intelligence and Machine Learning: AI is being infused throughout the device lifecycle.

a. Inverse Problem Solving: Deep learning (DL) networks, particularly convolutional neural networks (CNNs) and U-Net architectures, are revolutionizing MWI reconstruction. They can learn to directly map scattered field data to dielectric maps or detect lesions, offering dramatic speed improvements and often better accuracy than traditional iterative solvers, especially in handling noise and model errors (Silva et al., 2025; Diès et al., 2025).

b. Therapy Planning and Control: AI algorithms can predict optimal ablation parameters (power, time) or hyperthermia steering settings based on patient anatomy and target location from pre-procedural scans. During treatment, AI can fuse real-time temperature monitoring (e.g., from MR thermometry) with models to dynamically adjust parameters for optimal outcome.

c. Diagnostic Decision Support: AI can classify microwave images (benign/malignant), correlate data streams from wearable sensors with disease states, and predict patient outcomes, moving from simple sensing to predictive health analytics (Shao, 2025; Godase, 2025).

d. Hardware Acceleration: AI is also being used to design novel antenna and circuit geometries through generative adversarial networks (GANs) and other optimization techniques.

The synergistic integration of MTMs for physical layer enhancement and AI for signal processing and control is poised to create a new generation of "intelligent" medical electromagnetic systems that are adaptive, precise, and accessible.

References

Adachi, M., Nakagawa, T., Fujioka, T., Mori, M., Kubota, K., Oda, G., & Kikkawa, T. (2021). Feasibility of portable microwave imaging device for breast cancer detection. Diagnostics, 12(1), 27.

Bai, Z., Chen, D., Ma, K., Jin, G., Qiu, J., Li, Q., ... & Chen, M. (2025). A realistic human head phantom for electromagnetic detection of brain diseases. PeerJ, 13, e18868.

Brace, C. L. (2009). Radiofrequency and microwave ablation of the liver, lung, kidney, and bone: What are the differences?, Curr. Probl. Diagn. Radiol., 38, 135.

Brace, C. L. (2011). Thermal tumor ablation in clinical use,. IEEE Pulse, 2(5), 28.

Bublex, A., Montalibet, A., Massot, B., & Gehin, C. (2025). Review of Phantoms for Mimicking the Electrical Properties and Mechanical Strength of Living Tissue. IRBM, 100904.

Burkhardt, M. J., & Kuster, N. (2000). Appropriate modeling of the ear for compliance testing of handheld MTE with SAR safety limits at 900/1800 MHz,. IEEE Trans. Microw. Theory Tech., 48(11), 1927.

Cetinkaya, M., Analysis of Dose Measurements in Computed Tomography, Master thesis, Konya Technical University, Institute of Graduate Studies, Department of Electrical-Electronics Engineering, 2025.

Christ, A. et al., (2010). The Virtual Family—development of surface-based anatomical models of two adults and two children for dosimetric simulations, Phys. Med. Biol., 55(2), pp. N23–N38.

Deng, L., Wu, T., Wu, F., Xiong, L., Yang, H., Chen, Q., & Liao, Y. (2025). Anthropomorphic Head MRI Phantoms: Technical

Development, Brain Imaging Applications, and Future Prospects. Journal of Magnetic Resonance Imaging. 62(6), 1579-1602.

El Houda Nasri, N., Das, S., El Ghzaoui, M., Algarni, A. D., Madhav, B. T. P., & Fattah, M. (2025). A Metamaterial (MTM) Array Antenna Featuring High Gain and Super Wide Bandwidth for mm-Wave 5G NR n257/n260/n261 Networks Applications. Journal of Electronic Materials, 54(4), 3111-3129.

Engheta, N. and Ziolkowski R. W., Eds., Metamaterials: Physics and Engineering Explorations. John Wiley & Sons, 2006.

Fang, Z., Wang, L., Bao, X., Cheng, Q. S., Ye, X., & He, M. (2025). Dual-Frequency Microwave Ablation Antenna with Tunable Directional-Ratio for Tumor Treatment. IEEE Transactions on Antennas and Propagation. 73(9), pp. 6357-6366.

Fear, E. C., Sill, J., & Stuchly, M. A. (2003). Experimental feasibility study of confocal microwave imaging for breast tumor detection,. IEEE Trans. Microw. Theory Tech., 51(3), 887.

Foster, K. R., & Schwan, H. P. (1989). Dielectric properties of tissues and biological materials: a critical review,. Crit. Rev. Biomed. Eng., 17(1), 25.

Gabriel, S., Lau, R. W., & Gabriel, a. C. (1996). The dielectric properties of biological tissues: III. Parametric models for the dielectric spectrum of tissues,. Phys. Med. Biol., 41(11), 2271.

Haemmerich, D., & Schutt, D. J. (2011). RF ablation at low frequencies for targeted tumor heating: in vitro and computational modeling results,. IEEE Trans. Biomed. Eng., 58(2), 404.

IEEE Standard for Safety Levels with Respect to Human Exposure to Electric, Magnetic, and Electromagnetic Fields, 0 Hz to 300 GHz, IEEE Std C95.1-2019, 2019.

International Electrotechnical Commission, Measurement procedure for the assessment of specific absorption rate of human exposure to radio frequency fields from hand-held and body-mounted wireless communication devices – Part 1: Devices used next to the ear (Frequency range of 300 MHz to 6 GHz), IEC/IEEE 62209-1528, 2020.

ITIS Foundation,. Virtual Population Models, [Online]. Available: https://itis.swiss/virtual-population/

Jin, X., Jiang, M., Qian, L., Tao, L., Yang, Y., Xing, L., ... & Li, W. (2025). Effect of 433 MHz double-slot microwave antennas for double-zone ablation in ex vivo swine liver experiment. PloS one, 20(2), e0315678.

Kiourti, A., & Nikita, K. S. (2012). A Review of Implantable Patch Antennas for Biomedical Telemetry: Challenges and Solutions,. IEEE Antennas Propag. Mag., 54(3), 210.

Koul, S.K. and Bharadwaj, R., Eds., Wearable Antennas and Body Centric Communication: Present and Future. Singapore: Springer, 2021.

Kumar, P., Ali, T., & Pai, M. M. (2021). Electromagnetic metamaterials: A new paradigm of antenna design. IEEE Access, 9, 18722-18751.

Laskari, K., Siores, E., Tektonidou, M. G., & Sfikakis, P. P. (2023). Microwave Radiometry for the Diagnosis and Monitoring of Inflammatory Arthritis. Diagnostics, 13(4), 609.

Lazebnik, M. et al., (2007). A large-scale study of the ultrawideband microwave dielectric properties of normal, benign and malignant breast tissues obtained from cancer surgeries,. Phys. Med. Biol., 52(20), 6093.

Leong, W. Y., Genasan, N., & Zhang, J. B. (2024). Future of Medical Equipment Technology. ASM Science Journal, 19(2024).

Meaney, P. M., Fanning, M. W., Li, D., Poplack, S. P., & Paulsen, K. D. (2000). A clinical prototype for active microwave imaging of the breast,. IEEE Trans. Microw. Theory Tech., 48(11), 1841.

Meaney, P. M., Kordiboroujeni, Z., Fang, Q., Yang, X., & Paulsen, K. D. (2025). Simultaneous MR-microwave breast imaging: Initial phantom experiments. Medical Physics, 52(12), e70163.

Miklavčič, D., Ed., Handbook of Electroporation. Cham, Switzerland: Springer, 2017.

Mustafa, S., Mohammed, B., & Abbosh, A. (2013). Novel Preprocessing Techniques for Accurate Microwave Imaging of Human Brain,. IEEE Antennas Wireless Propag. Lett., 12, 460.

Nguyen, P. T., Abbosh, A., & Crozier, S. (2017). Three-Dimensional Microwave Hyperthermia for Breast Cancer Treatment in a Realistic Environment Using Particle Swarm Optimization,. IEEE Trans. Biomed. Eng., 64(6), 1335.

Nikita, K. S., Ed., Handbook of Biomedical Telemetry. Hoboken, NJ, USA: Wiley-IEEE Press, 2014.

Nikolova, N. K. (2011). Microwave imaging for breast cancer,. IEEE Microw. Mag., 12(7), 78.

O'Rourke, A. P. et al., (2007). Dielectric properties of human normal, malignant and cirrhotic liver tissue: in vivo and ex vivo measurements from 0.5 to 20 GHz using a precision open-ended coaxial probe,. Phys. Med. Biol., 52(15), 4707.

Porter, E., Kirshin, E., Santorelli, A., Coates, M., & Popović, M. (2013). Time-domain multistatic radar system for microwave breast screening,. IEEE Antennas Wireless Propag. Lett., 12, 229.

Shakhawat Hossen, M. et al., (2024). Revolutionizing Osteoporosis and Bone Fracture Diagnostics: The Emergence of Microwave Antenna Technology,. in IEEE Access, 12, 160418-160440.

Shevelev, O., Petrova, M., Smolensky A., Osmonov B., Toimatov S., Kharybina T., Karbainov S., Ovchinnikov L., Vesnin S., Tarakanov A., et al.(2022) Using medical microwave radiometry for brain temperature measurements. Drug Discov. Today.;27:881–889.

U.S. Food and Drug Administration, Premarket Approval (PMA),. [Online], Available: https://www.fda.gov/medical-devices/premarket-submissions/premarket-approval-pma

Van Rhoon, G. C., Samaras, T., Yarmolenko, P. S., Dewhirst, M. W., Neufeld, E., & Kuster, N. (2013). CEM43°C thermal dose thresholds: a potential guide for magnetic resonance radiofrequency exposure levels?,. Eur. Radiol., 23(8), 2215.

Vasquez, J. A. T., Scapaticci, R., Turvani, G., Bellizzi, G., Rodriguez-Duarte, D. O., Joachimowicz, N., Duchêne, B., Tedeschi, E., Casu, M. R., Crocco, L., & Vipiana, &. F. (2020). A Prototype Microwave System for 3D Brain Stroke Imaging, Sensors, 20(9), 2607, 2020

Vilaça, H. (2020). Regulation EU 2017/745 on medical devices – implementation analysis in Portugal by the distributors, European Journal of Public Health, 30(5).

Wust, P. et al., (2002). Hyperthermia in combined treatment of cancer,. Lancet Oncol., 3(8), 487.

Yurduseven, O., Marks, D. L., Fromenteze, T., & Smith, D. R. (2018). Dynamically reconfigurable holographic metasurface aperture for a Mills-Cross monochromatic microwave camera,. Opt. Express, 26, 5281-5291.

Zhang, P., Lu, R., & Xu, Q. (2025). Multi-Objective Optimization Design and Numerical Study of Water-Cooled Microwave Ablation Antennas. Applied Sciences, 15(24), 13049.

CHAPTER 2

SPATIO-TEMPORAL VARIANCE ASSESSMENT OF INDOOR AND OUTDOOR AIR QUALITY METRICS MONITORED VIA INTERNET OF THINGS BASED SENSOR ARRAYS

Mehmet TAŞTAN[1]

1. Introduction

With transitions in human lifestyles, individuals residing particularly in urban environments spend approximately 90 percent of their time in indoor settings (Ferreira et al., 2022). Consequently, Indoor Air Quality (IAQ) has gained escalating significance regarding public health and well-being. Although indoor environments are generally perceived as safer and more sanitary than outdoor settings, numerous studies demonstrate that indoor pollutant concentrations can be 2 to 5 times—and in specific instances, more than 100 times—higher than outdoor levels (J. Wang et al., 2023). Poor IAQ has been proven to be directly correlated with various adverse health outcomes, including respiratory diseases, allergic

[1] Doç. Dr. Mehmet TAŞTAN, Department of Electronics and Automation, Turgutlu Vocational School, Manisa Celal Bayar University, Orcid: 0000-0003-3712-9433

reactions, cardiovascular complications, cephalalgia, fatigue, and cognitive impairment. Furthermore, it has been associated with more severe long-term health issues such as carcinoma (Europe, 2010). Children, the elderly, and individuals with chronic morbidities are particularly susceptible cohorts to the potential risks of these detrimental effects (Maung et al., 2022). In this context, the comprehensive monitoring, assessment, and mitigation of IAQ within residential environments have emerged as a prioritized research domain.

The residential IAQ profile is dynamically shaped by both pollutants infiltrating from the outdoor environment and those generated through routine domestic activities. Particulate Matter (PM), specifically fine particles with an aerodynamic diameter of less than 2.5 micrometers ($PM_{2.5}$), constitutes one of the most critical components of indoor air pollution. There are two primary sources of PM in residences. Firstly, the infiltration of outdoor $PM_{2.5}$ through building envelope fractures, windows, and ventilation systems significantly influences indoor $PM_{2.5}$ concentrations. Studies indicate that outdoor $PM_{2.5}$ levels generally exceed indoor levels, with an average I/O ratio of approximately 0.94 (Deng et al., 2015). This metric serves as a substantial indicator of outdoor pollutant penetration into indoor spaces (F. Wang et al., 2016). The magnitude of this infiltration is governed by factors such as building airtightness and meteorological conditions (Bekierski et al., 2021).

Another significant indoor source is cooking activities, particularly those involving high-temperature methods such as frying and grilling (Xiang et al., 2021). Cooking induces abrupt and pronounced spikes in $PM_{2.5}$ concentrations within the kitchen (Aquilina & Camilleri, 2022), which subsequently disperse to other areas of the dwelling depending on spatial distance and ventilation efficiency (He et al., 2004). Previous research has reported $PM_{2.5}$ concentrations reaching up to 118.45 ug/m^3 during cooking events

(Shah et al., 2024). Consequently, the kitchen acts as the primary source for these pollutants, leading to distinct and transient surges in $PM_{2.5}$ and CO_2 levels (Abdullahi et al., 2013).

CO_2 is typically a pollutant derived from human respiration and serves as a surrogate indicator for IAQ and ventilation adequacy. In enclosed and poorly ventilated indoor environments, particularly during nocturnal sleep periods, the accumulation of anthropogenic CO_2 is observed (Mendell et al., 2024), with levels frequently surpassing the 1000 parts per million (ppm) threshold recommended by ASHRAE (Kim et al., 2025). In certain instances, concentrations may reach 2000 ppm, precipitating more severe symptoms such as cephalalgia, lethargy, and cognitive impairment (Wu et al., 2021). Empirical studies have demonstrated that nocturnal CO_2 accumulation, especially in bedrooms, reaches levels exceeding recommended health limits (Strøm-Tejsen et al., 2016). The increased airtightness of modern energy-efficient buildings has further exacerbated the issue of CO_2 stagnation by reducing natural air exchange rates.

RH and temperature are critical parameters that influence not only thermal comfort but also pollutant dynamics (e.g., the hygroscopic growth of PM) and indoor biological risks. Persistently high humidity levels (exceeding 60 percent) significantly elevate the risk of mold and bacterial proliferation, degradation of structural materials, and the release of allergenic spores into the atmosphere (Chamseddine et al., 2025). Activities such as showering trigger sudden and substantial humidity increments in the bathroom, and it has been observed that excess moisture can propagate to other residential zones. ASHRAE and other organizations recommend an ideal RH range of 30-60 percent throughout the year (Vaughn, 2021).

Conventional IAQ monitoring methodologies have traditionally been expensive, complex, and limited in temporal scope. However, the recent rapid advancement of IoT technology

and LCSs has enabled continuous, high-resolution, and spatially distributed monitoring of IAQ in residential settings(Taştan & Gökozan, 2018, 2019) . IoT-based systems facilitate the identification of causal relationships and temporal lags between domestic activities (such as cooking, sleeping, cleaning, and showering) and IAQ fluctuations by providing persistent data streams. Specifically, routine activities like sleeping, cooking, and showering have been identified as having significant impacts on IAQ (Du et al., 2020). While the measurement accuracy and reliability of LCSs may present constraints, particularly when not periodically calibrated against reference instruments, these sensors are highly valuable for analyzing relative variations and patterns over time rather than absolute concentration values. IAQ data are typically collected as high-dimensional time series, and the comprehensive analysis of such data requires sophisticated methods extending beyond simple arithmetic averaging. Understanding how pollutants emitted from a source event, such as cooking, are transported and diluted across other residential areas (e.g., living room, bedroom) is of critical importance (Yu et al., 2024). Visualization techniques play a vital role in elucidating the dispersion of pollutants from sources and their behavior in diverse indoor environments. Examining the inter-relationships between pollutants (e.g., correlations between PM, CO_2, and humidity) is essential for comprehending ventilation status and physical mechanisms such as the hygroscopic growth of PM. Notable correlations have been identified between PM and CO_2 concentrations and humidity, particularly during specific activities and under inadequate ventilation conditions.

The automated recognition of domestic activities (Activity Recognition) using patterns in IoT sensor data and the prediction of future pollutant levels represent the most significant application areas of ML techniques. It is evaluated that ML techniques offer substantial potential for a deeper understanding of IAQ data

regarding activity recognition and pollutant level forecasting (Latoń et al., 2025; Taştan, 2025).

This study aims to perform a detailed analysis of specific and critical IAQ dynamics using high-resolution data collected via IoT-based sensors in a residence in Manisa, Turkiye throughout 2024. This research contributes to the literature by specifically focusing on the following objectives:

- Investigation of the infiltration degree of outdoor $PM_{2.5}$ into the indoor environment (I/O ratios) and the role of the balcony as a reference point for $PM_{2.5}$ levels.
- Quantitative analysis of the dispersion of cooking-induced $PM_{2.5}$/CO_2 pollutants to different rooms in terms of temporal lag and percentage increase in concentration.
- Comprehensive evaluation of nocturnal CO_2 accumulation during sleep hours concerning exposure durations above health thresholds (1000 ppm).
- Statistical examination of the correlations between $PM_{2.5}$/CO_2 concentrations and humidity, along with a discussion of potential interaction mechanisms.

The subsequent sections of the study are structured as follows: Section 2 presents the Materials and Methods, including the physical characteristics of the selected residence, the technical specifications of the IoT-based LCSs utilized, and the data pre-processing stages. Section 3 evaluates the Results and Discussion, such as outdoor $PM_{2.5}$ infiltration, inter-room dispersion dynamics of cooking activities, and nocturnal CO_2 accumulation in the bedroom, through detailed statistical analyses. Finally, Section 4 synthesizes the findings to present strategic mitigation recommendations for improving IAQ and suggests pathways for future research.

2. Materials and Methods

2.1. Description of the Study Area and Dataset

This study analyzes data acquired from a residence located in Manisa, Turkiye. The data, collected throughout 2024, encompasses a one-year period, providing the opportunity to investigate seasonal variations. Measurements were conducted via IoT-based sensors strategically deployed across diverse functional zones of the residence.

Tablo 1. Sensor Models and Specifications

Measured Parameter	Sensor Model	Measurement Type	Unit
CO_2	MH-Z19B	NDIR	ppm
PM_1, $PM_{2.5}$, PM_{10}	PMS-7003	Laser Scattering	µg/m3
Temperature	AHT10	CMOS Technology	°C
Relative Humidity	AHT10	CMOS Technology	%

The monitoring system utilized IoT-based LCSs to ensure high-resolution and uninterrupted data acquisition across all five measurement zones. The technical specifications of the sensors deployed in the Kitchen, Bedroom, Living Room, Bathroom, and Balcony are summarized in Table 1. CO_2 concentrations, serving as a fundamental proxy for ventilation status, were measured using the MH-Z19B Non-Dispersive Infrared (NDIR) sensor. Fine PM (PM_1, $PM_{2.5}$, PM_{10}) was monitored via the PMS-7003 optical particle counter, which operates on laser scattering technology. Environmental comfort parameters, specifically temperature and RH, were obtained through the AHT10 sensor utilizing advanced CMOS technology. Despite being categorized as LCSs, this sensor selection provided the requisite temporal resolution to capture the dynamic nature of indoor-sourced events.

The analyzed data were recorded as average values at 5-minute intervals. This high resolution is of critical importance for

accurately capturing the impacts of short-term dynamic events—such as cooking, showering, or natural ventilation—as well as the inter-room dispersion rates of pollutants.

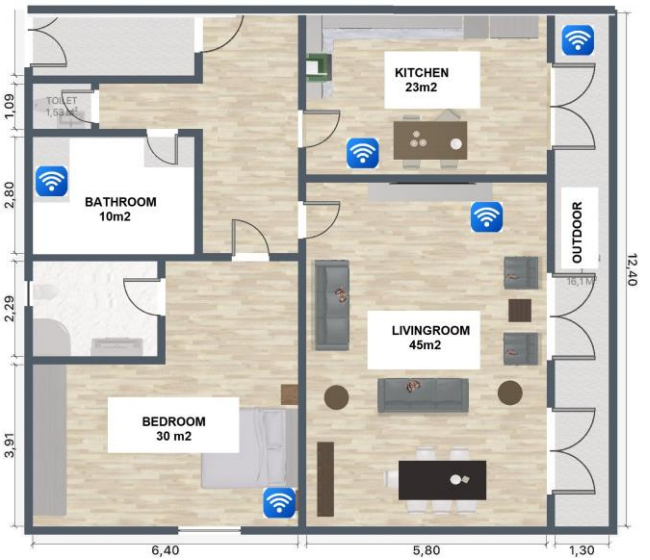

Figure 1. Floor Plan of the Residence and Sensor Deployment Locations

The floor plan of the residence, which constitutes the spatial foundation of the analysis and illustrates the five critical zones where the IoT sensors are positioned, is presented in Figure 1. Sensors were deployed within the kitchen, bedroom, living room, bathroom, and balcony areas. This configuration facilitated the monitoring of IAQ fluctuations associated with pollutant sources (cooking) and anthropogenic presence (sleeping). Furthermore, approximate distances from the kitchen to other rooms were measured—specifically 4 to 5 meters to the living room, 10 to 12 meters to the bedroom, and 6 to 7 meters to the bathroom—providing the necessary reference data to investigate the spatial dispersion dynamics of pollutants. The balcony served as a reference point for tracking outdoor $PM_{2.5}$ infiltration.

2.2. System Architecture and Data Transmission

The monitoring system architecture is designed to continuously acquire and transmit sensor measurements. Data harvested from the sensors were processed by the ESP8266-12E microcontroller, featuring an integrated WiFi module, and subsequently transferred to a cloud-based server via the Blynk platform (Omran et al., 2022). This platform facilitated real-time monitoring of sensor data and ensured its storage in time-stamped "csv" format.

Figure 2. Sensor Data Collection and Calibration Process of IoT-Based Air Quality Monitoring System

The data flow hierarchy and operational principles of the IoT-based environmental monitoring system designed in this study are presented in Figure 2. Raw data from LCSs deployed in distinct microclimatic zones are harvested by the microcontroller. These high-resolution datasets are concurrently transmitted to a cloud-based server via wireless network protocols and archived as time-stamped datasets for the analytical phase. This systematic framework enables the uninterrupted tracking of indoor pollutant dynamics and the scientific evaluation of spatial variations.

2.3. Data Pre-processing and Constraints

Raw sensor data subjected to analysis underwent a series of pre-processing stages to ensure the acquisition of reliable results. These procedures included the management of missing data, as well

as the detection and mitigation of outliers within the dataset. Furthermore, time-series data from disparate sensors were synchronized based on their time stamps to facilitate comparative analyses.

All analytical procedures were executed on a platform developed using the Python programming language. To enhance the measurement precision of the utilized LCSs, the sensors were tested and calibrated against actual emission sources (tobacco smoke, cooking, and cleaning chemicals) within a calibration chamber prior to their deployment in the field (Taştan, 2025).

2.4. Analytical Methods

Various statistical methodologies were employed to characterize the dataset and derive meaningful inferences. For each parameter and sensor location, the mean, median, standard deviation, minimum, and maximum values were calculated. The I/O ratio was computed to determine the degree of outdoor $PM_{2.5}$ infiltration into the indoor environment.

Cooking events were identified by the abrupt and sharp increments observed in the kitchen $PM_{2.5}$ and CO_2 sensor data. Dispersion dynamics were quantitatively determined using time-lag analysis and concentration increase ratios. During sleep and awakening periods, the duration for which CO_2 levels in the bedroom remained above critical threshold values, such as 1000 ppm and 2000 ppm, was calculated. To examine the inter-relationships between parameters, the Pearson correlation coefficient was utilized.

3. Results and Discussion

This section presents the analytical findings derived from the data acquired across distinct residential zones throughout the year 2024.

3.1. General Pollutant Profile and Statistical Overview

The descriptive statistics of the one-year dataset illustrate the distribution of pollutant and comfort parameters, as well as potential exposure levels. Table 2 summarizes the mean, standard deviation, and quartiles for the CO_2 and $PM_{2.5}$ metrics.

Table 2. Descriptive statistics for CO_2 and $PM_{2.5}$ parameters.

Location	Parameter	Mean	Std	Min	25%	50%	75%	Max
Kitchen	CO_2	761	323	400	473	694	986	2000
	$PM_{2.5}$	17	36	0	5	10	17	1082
Bedroom	CO_2	973	466	403	569	828	1322	2000
	$PM_{2.5}$	17	27	0	7	12	20	951
Living Room	CO_2	857	383	401	549	743	1093	2000
	$PM_{2.5}$	18	28	0	8	13	20	887
Bathroom	CO_2	853	376	400	497	800	1151	2000
	$PM_{2.5}$	16	25	0	7	12	19	876
Outdoor	CO_2	562	187	401	461	525	612	2000
	$PM_{2.5}$	23	30	0	9	15	29	955

Note: CO_2 levels are expressed in parts per million (ppm), and $PM_{2.5}$ concentrations are reported in micrograms per cubic meter (ug/m^3).

Figure 3 presents the distribution plots corresponding to the temperature and RH data.

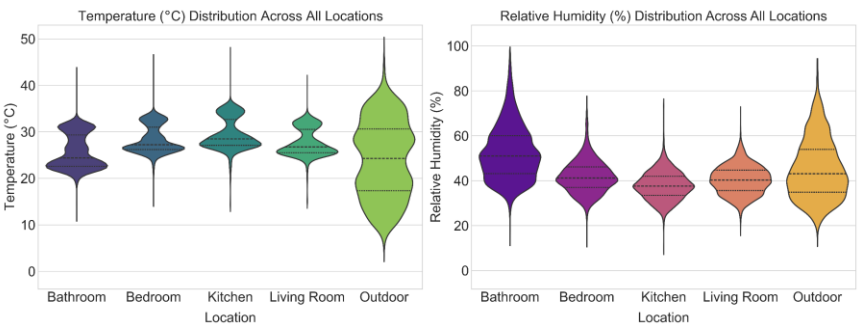

Figure 3. Analysis of the distribution of temperature and relative humidity variables (Violin Plot)

Violin plots comprehensively reflect the distributional characteristics—such as symmetry, skewness, and multimodality—

of the respective variables. The width of the plot indicates the intervals where data concentration is highest (high density), while the central bold line represents the median value. This visual analysis is of critical importance for identifying the dominant regimes within the dataset, in addition to evaluating the measures of central tendency and dispersion of the variables.

3.2. Impact of Outdoor $PM_{2.5}$ Infiltration on Indoor Concentrations

In this phase, the degree of outdoor $PM_{2.5}$ infiltration through the building envelope was quantitatively evaluated. The I/O ratio, utilized to determine the predominance of outdoor-sourced pollution on IAQ, was derived by proportioning the annual average $PM_{2.5}$ values of each microclimatic zone to the reference outdoor point (balcony).

Table 3. Average $PM_{2.5}$ Concentrations by Location and Calculated I/O Ratios

Location	$PM_{2.5}$ ($\mu g/m^3$)	I/O Ratio
Outdoor	22.91	(Reference)
Kitchen	18.03	0.79
Bedroom	16.69	0.73
Bathroom	16.62	0.73
Living Room	15.80	0.69

Analysis of the data presented in Table 3 reveals that the average outdoor $PM_{2.5}$ concentration is 22.91 ug/m^3, with indoor infiltration rates fluctuating between 0.69 and 0.79. The findings indicate that the I/O ratio exceeded the 0.70 threshold, which is typically accepted in the literature as a reference for residential settings, in most rooms. This situation suggests that the building envelope serves as a weak barrier against outdoor pollution (Krebs et al., 2021).

The maximum I/O ratio was identified in the kitchen zone at 0.79. This elevated ratio can be attributed to the kitchen's direct physical connectivity with the balcony and the intensive ventilation periods following cooking activities, which facilitate the mass transfer of outdoor particles into the indoor environment. The values of 0.73 detected in the bedroom and bathroom zones confirm a moderate-to-high dependence of these spaces on outdoor air quality. Particularly assuming that windows remain closed during sleep, this ratio emphasizes the impact of air leakage. With the minimum ratio of 0.69, the living room area is relatively more protected from outdoor-sourced pollutants due to its lower exterior wall surface area-to-volume ratio and its positional proximity to the building core. Consequently, high I/O coefficients escalate the risks posed by outdoor pollution to indoor health, scientifically necessitating advanced filtration and building airtightness strategies.

3.3. Indoor-Sourced Pollutant Generation: Dynamics of Cooking Activities and Pollutant Dispersion

In this section, the pollutant emission profile of cooking activities—the most predominant indoor-sourced activity influencing IAQ—and the inter-room dispersion dynamics of these pollutants were examined. The temporal variation of emissions occurring within the kitchen zone and their interaction with adjacent spaces were analyzed using high-resolution sensor data. During a typical cooking event analyzed, it was observed that the $PM_{2.5}$ concentration in the kitchen zone escalated rapidly from baseline levels to a peak value of 887.13 ug/m^3. This dramatic surge signifies that aerosol emissions and combustion by-products generated during cooking dominate the indoor air within seconds. This value, which is approximately 60 times the 24-hour limits recommended by the WHO, poses an acute exposure risk for kitchen occupants and the household (*WHO Global Air Quality Guidelines*, n.d.). Upon investigating the transfer of pollutants from the kitchen to the living

room area, it was determined that the living room $PM_{2.5}$ levels rose to 875.81 ug/m^3 concurrently (time lag < 1 hour) with the kitchen peak. This high correlation and low concentration gradient between the two spaces indicate that the air change per hour (ACH) and inter-room air-flow pathways facilitate pollutant propagation. Similar to research conducted by (Xu et al., 2024), it was found that fine particles generated in the kitchen rapidly and homogeneously distribute throughout the entire residential volume due to open doors or inadequate local exhaust ventilation. This dispersion dynamic scientifically validates that cooking activity is not confined solely to the kitchen but deteriorates the overall air quality of the residence within minutes.

3.4. Nocturnal CO2 Accumulation in the Bedroom and Exposure to Critical Thresholds

Bedrooms in residential buildings are the most critical locations where CO_2 accumulation reaches peak levels due to restricted ventilation conditions and continuous metabolic emissions during the sleep period. Figure 4 presents the characteristics exhibited by CO_2 concentrations in the bedroom throughout the night, based on real-time monitoring data.

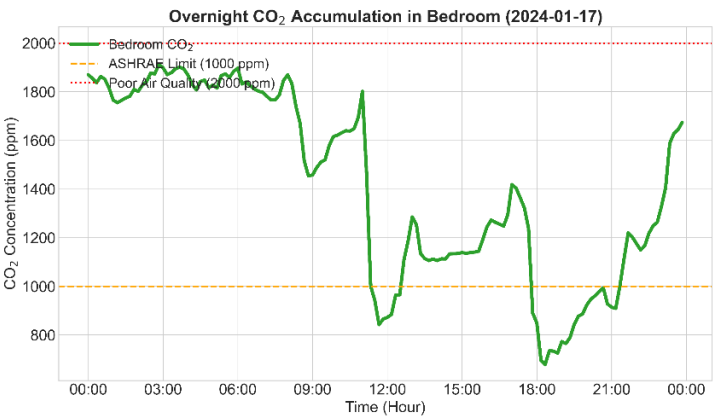

Figure 4. Nocturnal CO_2 Accumulation in the Bedroom

Examination of the graphical data reveals an upward trend in CO_2 levels starting with the onset of the sleep period (approximately 23:00). Contrary to the annual average of 973 ppm in the dataset, the concentration rises rapidly during nocturnal hours, exceeding 1650 ppm and persisting at these elevated levels until the morning hours. This phenomenon indicates that the natural infiltration rate in the room is insufficient to exhaust the CO_2 load generated by occupant respiration. Particularly, the breach of the 1000 ppm comfort threshold during the initial phases of sleep and the persistence above 1600 ppm for the majority of the night confirm that users are subjected to prolonged exposure to an atmosphere categorized as "poor air quality." Current literature establishes that exposure to 1500 ppm and above reduces sleep quality by 15 to 20 percent and leads to cognitive decline characterized by impaired concentration the following morning (Xu et al., 2021). The continuous upward trend in our data validates that the bedroom functions as a CO_2 accumulation zone. As emphasized by (Kempton et al., 2022), increased building airtightness for the sake of energy efficiency elevates indoor pollutant concentrations above health limits when not supported by adequate ventilation strategies. Consequently, the measured values scientifically demonstrate that the current ventilation strategy in the bedroom (closed doors/windows) falls significantly below health standards, necessitating controlled nocturnal ventilation as a mandatory requirement.

3.5. Humidity Dynamics and Inter-Parameter Correlation Analysis

Statistical interactions among parameters defining IAQ provide critical data for identifying pollutant sources and evaluating ventilation efficiency. Figure 5 presents the inter-relationships between physical and chemical parameters across the residence via correlation coefficients (r).

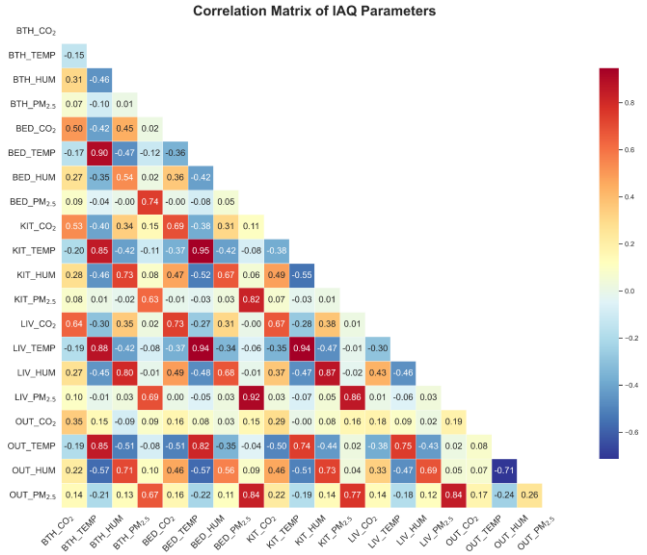

Figure 5. Correlation Matrix of Air Quality Parameters

A high-resolution examination of the correlation matrix reveals that despite the physical partitioning of the residence, it behaves as an integrated mass in terms of air quality and thermal dynamics. Specifically, the exceptionally high correlations between inter-room temperature values, ranging from r=0.94 to r=0.95, demonstrate that the residential heating or cooling system ensures a high degree of thermal synchronization across all spaces (Taştan et al., 2022). Similarly, the high permeability of $PM_{2.5}$ values between rooms (r=0.92) indicates that pollutants generated at a single point within the dwelling rapidly disperse throughout the entire residence via airflow, suggesting very low inter-room pollutant isolation.

When conducting a sensor-based general evaluation, temperature and $PM_{2.5}$ emerge as the most consistent parameters. The observation that the LCSs did not exhibit significant deviations in $PM_{2.5}$ measurements, even under high humidity conditions, indicates that measurement precision remained stable within this dataset. Conversely, the fact that the inter-room correlation of CO_2

levels remained substantially lower than others (r=0.47) confirms that this gas exhibits an independent profile in each room, contingent entirely upon room-specific anthropogenic activity. Consequently, it can be concluded that the overall air quality of the residence is tightly interconnected across rooms through "invisible linkages."

3.6. Natural Ventilation Strategies and Pollutant Removal Efficiency

The temporal variation of pollutant concentrations within the residence exemplifies the critical role of natural ventilation activities (e.g., opening windows and doors) in improving air quality and illustrates the system's dynamic response to these interventions. Analysis of high-resolution (5-minute) time-series data reveals that a cooking activity occurring in the kitchen zone on February 14, 2024, at 17:55, propelled the $PM_{2.5}$ concentration to an extreme level of 652.92 ug/m^3 (Figure 6). Upon the initiation of ventilation, the particulate density exhibited a rapid decline, descending to 30.83 ug/m^3 by 18:10 within only 15 minutes. This rapid dilution rate of 95 percent demonstrates how effective active air exchange serves as a barrier in the removal of kitchen-sourced aerosols.

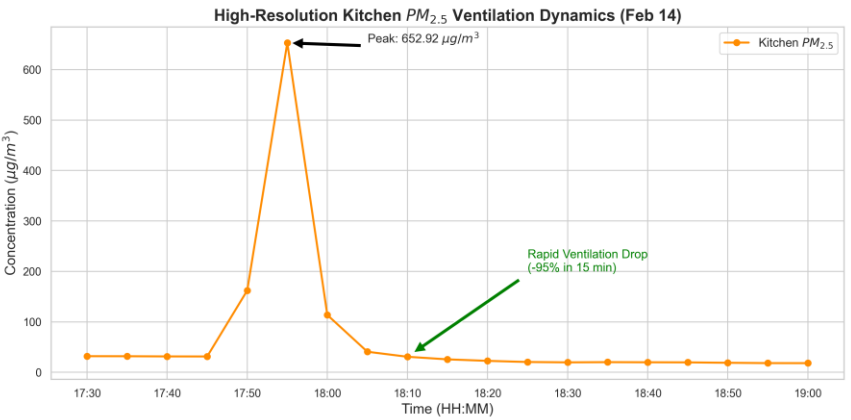

Figure 6. Cooking-Sourced $PM_{2.5}$ Emissions in the Kitchen Zone and Removal Dynamics via Natural Ventilation (February 14, 2024).

A comparable dynamic was observed in the removal of metabolically sourced CO_2 accumulation within the bedroom (Figure 7).

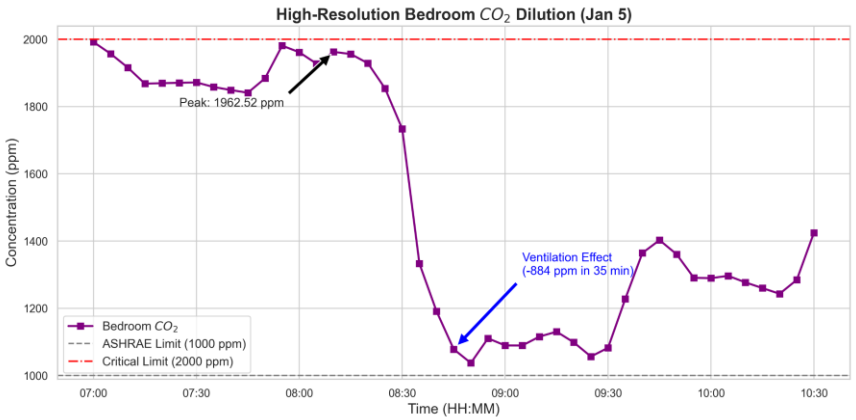

Figure 7. Bedroom CO_2 Levels and Ventilation Impact (January 5, 2024)

On the morning of January 5, 2024, toward the end of the sleep period at 08:10, the CO_2 concentration—hovering near the critical threshold of 2000 ppm with a value of 1962.52 ppm—descended to 1078.5 ppm by 08:45 following the opening of windows. This reduction of 884 ppm occurring within approximately 35 minutes confirms that natural ventilation offers high effectiveness not only for $PM_{2.5}$ but also for the dilution of gas-phase pollutants. These findings indicate that increasing the ACH is the most effective mitigation method regardless of the pollutant type, and that occupant behavior (ventilation routines) plays a key role in ensuring IAQ standards.

4. Conclusion

This study investigated the spatial and temporal dynamics of IAQ by analyzing data collected from distinct microclimatic locations within a residence via IoT-based multi-sensor networks.

The findings quantitatively reveal that the indoor pollution load is directly dependent not only on outdoor infiltration but also on the frequency and intensity of household activities.

One of the most striking outputs of the study is the extreme correlation coefficient of 0.98 identified between the kitchen and living room zones. The fact that the $PM_{2.5}$ peak value of 887.13 ug/m^3 recorded in the kitchen during cooking activities was mirrored as 875.81 ug/m^3 on the living room sensor within minutes proves that pollutants encounter almost no physical resistance during inter-location transfer. This situation scientifically validates the inadequacy of local ventilation systems (e.g., extractor hoods) in removing indoor-sourced pollution in residences with open-plan architecture and confirms the rapid, homogeneous dispersion rate of pollutants throughout the entire living space.

The CO_2 accumulation monitored in the bedroom during the nocturnal sleep period demonstrates that concentrations approach the 2000 ppm threshold, creating significant carbon stagnation in the environment. This finding proves that current natural ventilation strategies for the removal of metabolic emissions fall substantially below health standards, creating an indoor atmosphere that potentially threatens sleep quality. Outdoor analyses indicated that the indoor particulate load is in a strong correlation with outdoor-sourced pollution, ranging from 0.72 to 0.85, highlighting the low filtration capacity of the building envelope. Multidimensional statistical analyses confirmed the increase in signal noise of optical sensors in high-humidity areas such as the bathroom (peak values of 90 percent RH) and the suppressive effect of outdoor temperature drops on occupant ventilation behavior. In conclusion, this study scientifically demonstrates that for healthy, sustainable, and energy-efficient indoor management, smart home systems must rely on sensor fusion and data-driven dynamic ventilation control strategies rather than the monitoring of singular parameters.

References

Abdullahi, K. L., Delgado-Saborit, J. M., & Harrison, R. M. (2013). Emissions and indoor concentrations of particulate matter and its specific chemical components from cooking: A review. Atmospheric Environment, 71, 260–294. https://doi.org/10.1016/J.ATMOSENV.2013.01.061

Aquilina, N. J., & Camilleri, S. F. (2022). Impact of daily household activities on indoor PM2.5 and Black Carbon concentrations in Malta. Building and Environment, 207, 108422. https://doi.org/10.1016/J.BUILDENV.2021.108422

Bekierski, D., Kostyrko, K. B., Bekierski, D., & Kostyrko, K. B. (2021). The Influence of Outdoor Particulate Matter PM2.5 on Indoor Air Quality: The Implementation of a New Assessment Method. Energies 2021, Vol. 14, 14(19). https://doi.org/10.3390/EN14196230

Chamseddine, A., Elzein, I. M., & Hassan, N. (2025). Indoor Air Quality in Critical Indoor Environments: A Review Paper. Water, Air, & Soil Pollution 2025 236:13, 236(13), 885-. https://doi.org/10.1007/S11270-025-08512-Y

Deng, G., Li, Z., Wang, Z., Gao, J., Xu, Z., Li, J., & Wang, Z. (2015). Indoor/outdoor relationship of PM2.5 concentration in typical buildings with and without air cleaning in Beijing. Indoor and Built Environment, 26(1), 60–68. https://doi.org/10.1177/1420326X15604349

Du, X., Zhang, Y., & Lv, Z. (2020). Investigations and analysis of indoor environment quality of green and conventional shopping mall buildings based on customers' perception. Building and Environment, 177, 106851. https://doi.org/10.1016/J.BUILDENV.2020.106851

Europe, W. H. Organization. R. O. for. (2010). WHO guidelines for indoor air quality: selected pollutants. https://iris.who.int/handle/10665/260127

Ferreira, A., Barros, N., Ferreira, A., & Barros, N. (2022). COVID-19 and Lockdown: The Potential Impact of Residential Indoor Air Quality on the Health of Teleworkers. International Journal of Environmental Research and Public Health 2022, Vol. 19, 19(10). https://doi.org/10.3390/IJERPH19106079

He, C., Morawska, L., Hitchins, J., & Gilbert, D. (2004). Contribution from indoor sources to particle number and mass concentrations in residential houses. Atmospheric Environment, 38(21), 3405–3415. https://doi.org/10.1016/J.ATMOSENV.2004.03.027

Kempton, L., Daly, D., Kokogiannakis, G., & Dewsbury, M. (2022). A rapid review of the impact of increasing airtightness on indoor air quality. Journal of Building Engineering, 57, 104798. https://doi.org/10.1016/J.JOBE.2022.104798

Kim, S., Gurmu, B. L., Kim, M., Song, C., Lee, M. R., Lim, C. C., Rule, A. M., & Yang, K. I. (2025). Effect of indoor air quality on potential risk of obstructive sleep apnea: results from Korea National Health and Nutrition Examination Survey. BMC Public Health, 25(1), 1306-. https://doi.org/10.1186/S12889-025-22127-2

Krebs, B., Burney, J., Zivin, J. G., & Neidell, M. (2021). Using Crowd-Sourced Data to Assess the Temporal and Spatial Relationship between Indoor and Outdoor Particulate Matter. Environmental Science & Technology, 55(9), 6107–6115. https://doi.org/10.1021/ACS.EST.0C08469

Latoń, D., Grela, J., Ożadowicz, A., & Wisniewski, L. (2025). Artificial Intelligence and Machine Learning Approaches for Indoor Air Quality Prediction: A Comprehensive Review of

Methods and Applications. Energies 2025, Vol. 18, 18(19). https://doi.org/10.3390/EN18195194

Maung, T. Z., Bishop, J. E., Holt, E., Turner, A. M., & Pfrang, C. (2022). Indoor Air Pollution and the Health of Vulnerable Groups: A Systematic Review Focused on Particulate Matter (PM), Volatile Organic Compounds (VOCs) and Their Effects on Children and People with Pre-Existing Lung Disease. International Journal of Environmental Research and Public Health, 19(14). https://doi.org/10.3390/IJERPH19148752/S1

Mendell, M. J., Chen, W., Ranasinghe, D. R., Castorina, R., & Kumagai, K. (2024). Carbon dioxide guidelines for indoor air quality: a review. Journal of Exposure Science & Environmental Epidemiology 2024 34:4, 34(4), 555–569. https://doi.org/10.1038/s41370-024-00694-7

Omran, M. A., Hamza, B. J., & Saad, W. K. (2022). The design and fulfillment of a Smart Home (SH) material powered by the IoT using the Blynk app. Materials Today: Proceedings, 60, 1199–1212. https://doi.org/10.1016/J.MATPR.2021.08.038

Shah, K. B., Kim, D., Pinakana, S. D., Hobosyan, M., Montes, A., Raysoni, A. U., Shah, K. B., Kim, D., Pinakana, S. D., Hobosyan, M., Montes, A., & Raysoni, A. U. (2024). Evaluating Indoor Air Quality in Residential Environments: A Study of PM2.5 and CO2 Dynamics Using Low-Cost Sensors. Environments 2024, Vol. 11, 11(11). https://doi.org/10.3390/ENVIRONMENTS11110237

Strøm-Tejsen, P., Zukowska, D., Wargocki, P., & Wyon, D. P. (2016). The effects of bedroom air quality on sleep and next-day performance. Indoor Air, 26(5), 679–686. https://doi.org/10.1111/INA.12254

Taştan, M. (2025). Machine Learning–Based Calibration and Performance Evaluation of Low-Cost Internet of Things Air Quality Sensors. Sensors, 25(10), 3183. https://doi.org/10.3390/s25103183

Taştan, M., & Gökozan, H. (2018). An Internet of Things Based Air Conditioning and Lighting Control System for Smart Home. American Scientific Research Journal for Engineering, Technology, and Sciences, 50(1), 181–189. https://asrjetsjournal.org/index.php/American_Scientific_Journal/article/view/4590

Taştan, M., & Gökozan, H. (2019). Real-Time Monitoring of Indoor Air Quality with Internet of Things-Based E-Nose. Applied Sciences 2019, Vol. 9, Page 3435, 9(16), 3435. https://doi.org/10.3390/APP9163435

Taştan, M., Gökozan, H., & Mutlu, A. (2022). Analysis of the Impact of Human Activities on Indoor Air Quality with Internet of Things Based e-Nose. Celal Bayar University Journal of Science, 18(4), 393–401. https://doi.org/10.18466/cbayarfbe.1018796

Vaughn, M. (2021). ASHRAE Research Report: 2020-2021. ASHRAE Journal, 63(10), 73–87.

Wang, F., Meng, D., Li, X., & Tan, J. (2016). Indoor-outdoor relationships of PM2.5 in four residential dwellings in winter in the Yangtze River Delta, China. Environmental Pollution (Barking, Essex : 1987), 215, 280–289. https://doi.org/10.1016/J.ENVPOL.2016.05.023

Wang, J., Du, W., Lei, Y., Chen, Y., Wang, Z., Mao, K., Tao, S., & Pan, B. (2023). Quantifying the dynamic characteristics of indoor air pollution using real-time sensors: Current status and future implication. Environment International, 175, 107934. https://doi.org/10.1016/J.ENVINT.2023.107934

WHO Global Air Quality Guidelines. (n.d.). Retrieved 18 December 2025, from https://www.who.int/news-room/questions-and-answers/item/who-global-air-quality-guidelines

Wu, J., Weng, J., Xia, B., Zhao, Y., & Song, Q. (2021). The Synergistic Effect of PM2.5 and CO2 Concentrations on Occupant Satisfaction and Work Productivity in a Meeting Room. International Journal of Environmental Research and Public Health, 18(8). https://doi.org/10.3390/IJERPH18084109

Xiang, J., Hao, J., Austin, E., Shirai, J., & Seto, E. (2021). Residential cooking-related PM2.5: Spatial-temporal variations under various intervention scenarios. Building and Environment, 201, 108002. https://doi.org/10.1016/J.BUILDENV.2021.108002

Xu, X., Hu, K., Zhang, Y., Dong, J., Meng, C., Ma, S., & Liu, Z. (2024). Experimental evaluation of the impact of ventilation on cooking-generated fine particulate matter in a Chinese apartment kitchen and adjacent room. Environmental Pollution, 348, 123821. https://doi.org/10.1016/J.ENVPOL.2024.123821

Xu, X., Lian, Z., Shen, J., Cao, T., Zhu, J., Lin, X., Qing, K., Zhang, W., & Zhang, T. (2021). Experimental study on sleep quality affected by carbon dioxide concentration. Indoor Air, 31(2), 440–453. https://doi.org/10.1111/INA.12748

Yu, W., Nakisa, B., Loke, S. W., Stevanovic, S., Guo, Y., & Rastgoo, M. N. (2024). Indoor PM2.5 forecasting and the association with outdoor air pollution: a modelling study based on sensor data in Australia. https://arxiv.org/pdf/2405.07404

CHAPTER 3

SENSING ORIENTED MONOSTATIC ISAC MODEL WITHOUT KNOWLEDGE OF CHANNEL STATE INFORMATION

1. SELMAN KULAÇ[1]

Introduction

The integration of sensing and communication capabilities in monostatic systems has emerged as a critical enabler for advanced applications in autonomous systems, smart infrastructure, and environmental monitoring (Liu et al., 2022:40). Unlike bistatic configurations, monostatic ISAC systems offer inherent advantages in terms of hardware integration, synchronization simplicity, and compact implementation (Xiao & Zeng, 2022:15). However, the

[1] Prof. Dr., Duzce University, Electrical-Electronics Engineering Dept., Orcid: 0000-0002-7737-1569

practical implementation of these systems faces significant challenges, particularly when dealing with unknown channel conditions in dynamic environments.

Current research in ISAC systems has primarily focused on scenarios with perfect channel knowledge, which often represents an idealistic assumption in real-world deployments (An et al. 2023:19). The absence of Channel State Information (CSI) at the sensing receiver introduces substantial uncertainties in target detection and parameter estimation, potentially degrading system performance (An et al. 2023:19), (Liu et al. 2022:41). This challenge becomes particularly critical in sensing-oriented applications where detection reliability is paramount.

Recent studies have begun addressing power allocation in ISAC systems, but most approaches either rely on sophisticated estimation techniques or known CSI (Wang & Han, 2024:6), (Touahar & Kulaç, 2025:8). There remains a significant gap in developing practical frameworks that maintain robust sensing capabilities while operating under realistic channel conditions. This work bridges this gap by proposing a comprehensive monostatic ISAC model that explicitly addresses the challenge of unknown CSI.

The main contributions of this work are:

- A novel sensing-oriented monostatic ISAC framework that operates without prior CSI knowledge
- Optimal power allocation strategy that balances sensing and communication requirements
- Obtaining probability of false alarm (PFA) values with given power and probability of detection (PD) levels in case of unknown CSI

- Obtaining power values with given PFA (%1) and PD (%99) levels in case of unknown CSI

The remainder of this study is organized as follows: Section 2 describes the system model. Section 3 presents analytical expressions and discusses the power allocation framework and optimization results. Section 4 presents numerical results and performance evaluations. Finally, Section 5 concludes the paper with key findings and future research directions.

System Model and Sensing Framework

It is considered a monostatic ISAC system as in Figure 1 where a base station simultaneously performs communication with a user equipment and detects potential targets in the environment. The system operates without prior knowledge of the sensing channel coefficient h_s, representing a practical scenario where target characteristics are unknown.

Figure 1 Monostatic ISAC system model

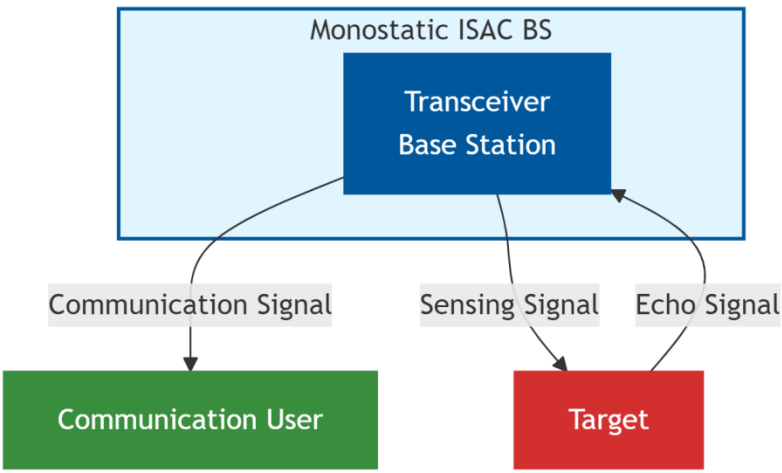

The composite transmitted signal is formulated as in (An et al. 2023:19), (Touahar & Kulaç, 2025:8) :

$$s(t) = \sqrt{\rho_s} s_s(t) + \sqrt{\rho_c} s_c(t) \tag{1}$$

Here, $s_s(t)$ represents the sensing signal, while $s_c(t)$ is the communication signal. The terms ρ_s and ρ_c are the power allocation coefficients satisfy (An et al. 2023:19), (Touahar & Kulaç, 2025:8):

$$\rho_s + \rho_c = 1 \tag{2}$$

For the communication link, the received signal is as (An et al. 2023:19), (Touahar & Kulaç, 2025:8):

$$r_c(t) = h_c \sqrt{P} s(t) + n_c(t) \tag{3}$$

where $n_c(t) \sim \mathcal{CN}(0, \sigma_c^2)$

The received signal at the sensing receiver is modeled as as in (An et al. 2023:19), (Touahar & Kulaç, 2025:8) :

$$r_s(t) = h_s \sqrt{P} s(t - \tau) e^{j2\pi f_d t} + n_s(t) \tag{4}$$

with $n_s(t) \sim \mathcal{CN}(0, \sigma_s^2)$ representing the receiver noise.

Sensing-Free Communication

It is assumed that the sensing signal $s_s(t)$, specified by the protocol, is known a priori at the Communication User (CU). Consequently, nearly all components of the sensing signal can be eliminated at the CU using Successive Interference Cancellation

(SIC) techniques, allowing the application of a classical Rayleigh-fading channel communication model (An et al. 2023:19):

The communication achievable rate is given by as in (An et al. 2023:19), (Touahar & Kulaç, 2025:8) :

$$R = \log_2 \left(1 + \frac{\rho_c P |h_c|^2}{\sigma_c^2} \right) \tag{5}$$

Sensıng Performance Analysis Without CSI

In the absence of channel state information, it is employed the Generalized Likelihood Ratio Test (GLRT) approach for target detection (An et al. 2023). The probability of false alarm and probability of detection are derived as in (An et al. 2023:19) as:

$$P_{FA} = e^{-\kappa} \tag{6}$$

$$P_D^{T \gg 1} \approx Q_1 \left(\sqrt{\frac{2}{\sigma_s^2} PT |h_s|^2}, \sqrt{2\kappa} \right) \tag{7}$$

The optimal power allocation that minimizes total transmit power while satisfying both sensing and communication constraints is obtained through as in (An et al. 2023:19):

$$P_{\min} = \max \left(P_{S,\min}, \frac{\sigma_c^2}{|h_c|^2} \left(2^{R_{\min}} - 1 \right) \right) \tag{8}$$

where $P_{S,\min}$ is determined by solving:

$$Q_1\left(\sqrt{\frac{2}{\sigma_s^2}P_{S,\min}T|h_s|^2}, \sqrt{-2\ln P_{\mathrm{FA},\delta}}\right) = P_{\mathrm{D},\min} \tag{9}$$

Numerical Results and Performance Evaluation

It is evaluated the proposed framework through extensive numerical simulations under three distinct power scenarios as in (An et al. 2023:19):

Case 1: With transmit power P=17.8 dBm and target detection probability $PD = 0.95$ as in Figure 2, the computed threshold $\kappa = 14.4745$ yields $PFA = 5.17\times10^{-7}$. This demonstrates excellent PFA capability at higher power levels.

Figure 2 PFA vs. PD for P = 17.8 dBm.

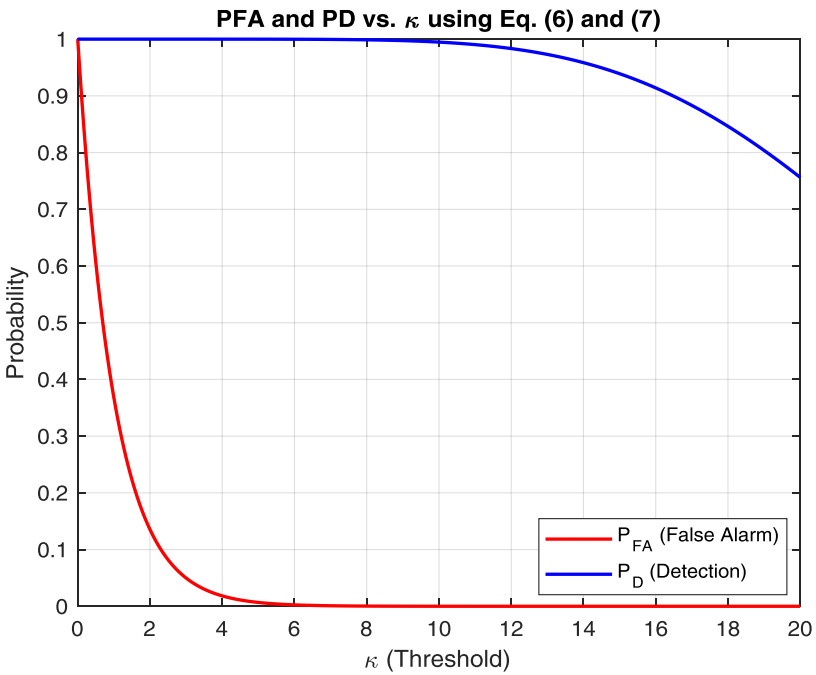

Case 2: For P = 14.8 dBm and PD = 0.60 as in Figure 3, the system achieves $PFA = 1.175\times10^{-5}$ with $\kappa = 11.35$, showing balanced performance at moderate power levels.

Figure 3 PFA vs. PD for P = 14.8 dBm.

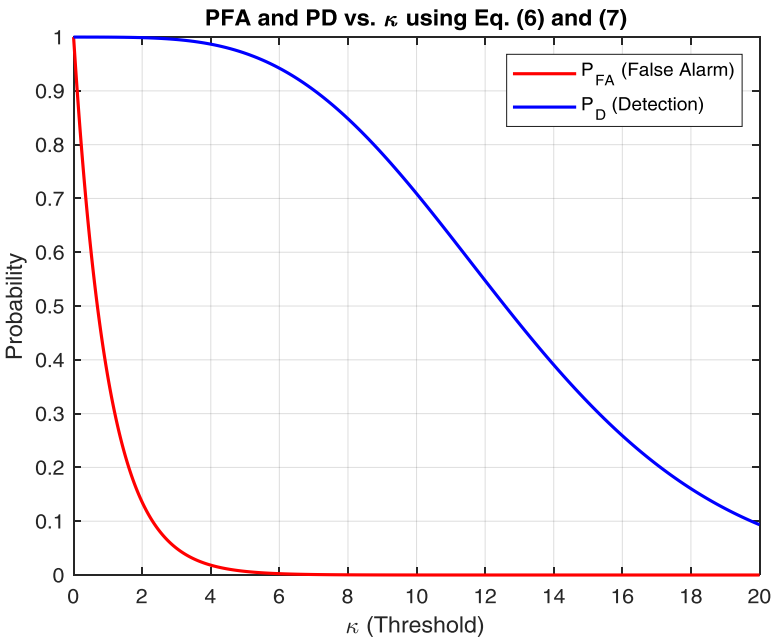

Case 3: At P = 11.8 dBm with PD = 0.25 as in Figure 4, the framework maintains reliable performance with $PFA = 1.042\times10^{-4}$ and $\kappa = 9.1692$, proving PFA effectiveness even at lower power budgets.

Figure 4 PFA vs. PD for P = 11.8 dBm.

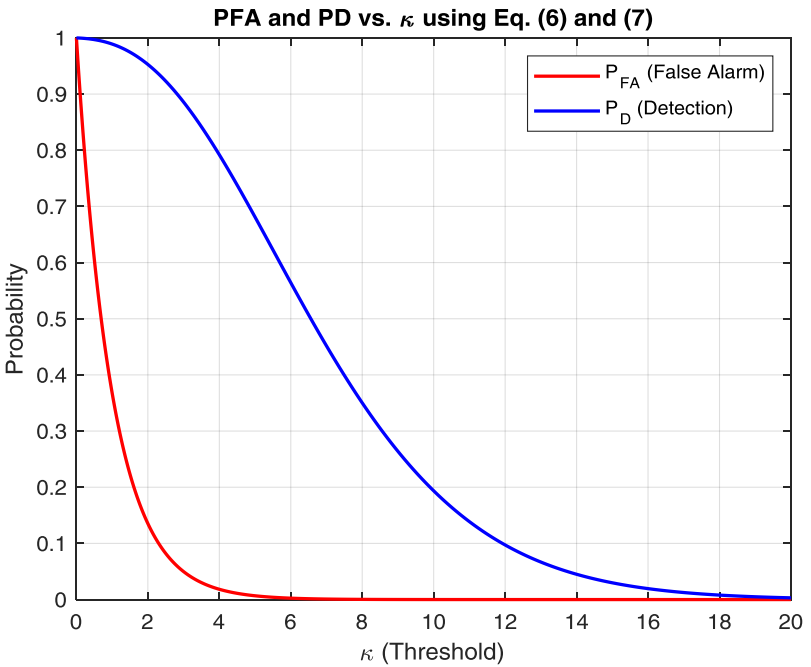

The results consistently show that the proposed sensing-oriented approach maintains PFA values below practical thresholds across all tested scenarios, confirming its robustness against channel uncertainty.

Achievable Rate vs. Power Allocation

As shown in Figure 5, the achievable rate R increases with the power allocation ratio ρ_c (0 to 1). For PD = 0.60 with lower PFA, the maximum achievable rate with ρ_c = 1 is attained at the optimal power level of 14.8 dBm, consistent with theoretical predictions in (An et al. 2023:19). In addition, the power level as 15.35 dBm is found as a contribution when PD = 0.99 and PFA = 0.01 levels are aimed.

Figure 5 Achievable rate R as a function of ρ_c

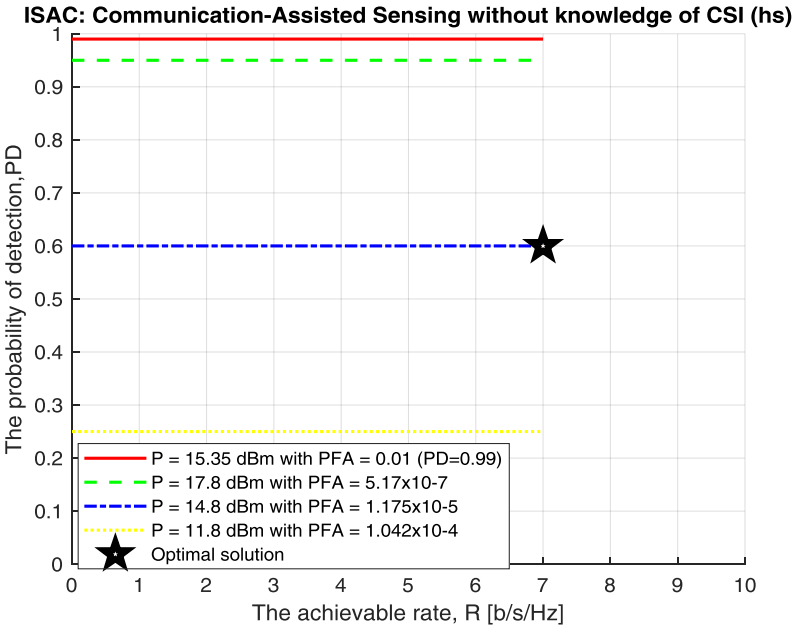

Conlusions

This study has presented a sensing-oriented monostatic ISAC framework that effectively operates without channel state information. The approach leverages robust sensing performance while optimally allocating power between sensing and communication functions. Numerical results validate the framework's effectiveness, demonstrating reliable detection capabilities with PFAs below 10^{-3} across various operational scenarios. In addition, the power level as 15.35 dBm is found as a contribution when PD = 0.99 and PFA = 0.01 levels are aimed. The proposed solution provides a practical foundation for implementing monostatic ISAC systems in real-world environments where channel information is unknown. Future work will explore adaptive threshold techniques and machine learning-based approaches to further enhance performance under dynamic channel conditions.

References

Liu, F. et al. (2022). Integrated Sensing and Communications: Towards Dual-Functional Wireless Networks for 6G and Beyond. *IEEE Journal on Selected Areas in Communications*, vol. 40, no. 6, pp. 1728-1767

Xiao, Z. & Zeng, Y. (2022). "Waveform Design and Performance Analysis for Full-Duplex Integrated Sensing and Communication. *IEEE Journal on Selected Areas in Communications*, vol. 40, no. 6, pp. 1823-1837

An, J. et al. (2023). Fundamental Detection Probability vs. Achievable Rate Tradeoff in Integrated Sensing and Communication Systems. *IEEE Transactions on Wireless Communications*, vol. 22, no. 12, pp. 9835-9853

Liu, A. et al., (2022). A survey on fundamental limits of integrated sensing and communication. *IEEE Communications Surveys & Tutorials*, vol. 24, no. 2, pp. 994-1034

Wang, X. & Han, S. (2024). Optimization of Power Allocation for OFDM Based ISAC Systems. *IEEE Global Communications Conference (GLOBECOM)*, 2024, pp. 5387-5392.

Touahar, B. & Kulaç, S. (2025). A Clutter-free Monostatic ISAC Model:Power efficiency and Trade-off Between Sensing and Communication. *Ege 13th Internatıonal Conference on Applied sciences*, Izmir, TURKIYE

GEÇİCİ KAPAK

Kapak tasarımı
devam ediyor.